Dust and Gas in NGC3627

Dust and Gas in NGC3627 Using Observations from SCUBA-2

By

Jonathan H. Newton, B.A.

A Thesis

Submitted to the School of Graduate Studies

in Partial Fulfilment of the Requirements

for the Degree

Master of Science

McMaster University

Master of Science (2014) McMaster University

(Physics and Astronomy) Hamilton, Ontario

TITLE: Dust and Gas in NGC3627 Using Observations from SCUBA-2

AUTHOR: Jonathan Newton, B.A. (Western Kentucky University)

SUPERVISOR: Christine D. Wilson

NUMBER OF PAGES: ix, 27

Abstract

Saw some dust and wanted to do something about it!

To my family and Poly.

Acknowledgements

When life looks like easy street, there is danger at your door... -Robert Hunter

Thank Chris and group members of course. Don't forget Christian!

Table of Contents

List of Figures

List of Tables

Chapter 1

Hello

Chapter 2

Observations and Data Preparation

2.1 SCUBA-2

The Submillimetre Common-User Bolometer Array 2 (SCUBA-2) was designed to decrease the observing time compared its predecessor SCUBA to allow for rapid data acquisition in the submillimetre regime of the electromagnetic spectrum, at the 450μm and 850μm bands with a 32μm and 85μm bandpass Holland et al. (2013). Prior to SCUBA-2, other bolometer camera's such as LABOCA, BOLOCAM and SHARC-II were limited to less than 100 pixels, while the new SCUBA-2 has been able to incorporate over 10,000 pixels in its design and effectively reduce observing time. Increasing the amount of pixels by a factor of 100 was possible by the advent of new technology such as high precision micromachining, superconducting transition edge sensors, and superconducting quantum interference device amplifiers (SQUIDs) Holland et al. (2013).

The observations of NGC3627 were taken from the Nearby Galaxies Legacy Survey's (NGLS) initial science images using SCUBA-2 from December 29,

2011 to January 21, 2012, and consist of 24 18‘x18‘ scans taken in grade 3 weather or better ($0.08 < \tau < 0.12$). 16 of the 24 scans were deemed useable, and whether or not an observation was deemed worthwhile was determined by factors such as the behavior of the image background or whether the image was flagged in observing to be unusable. The observations of NGC3627 were taken using a daisy scanning pattern at 150“/second in order to reduce the white noise of the final data product.

2.2 Image Creation and Properties

For any imaging process to have been successful, the image needed to have limited white noise (Chapin et al. (2013)). White noise in the sense of our bolometer observations arose from thermal variations in the instrument and atmosphere during data acquisition. The random noise can be minimized through scanning methods and during image processing Chapin et al. (2013). To create the final SCUBA-2 data products we used the Submillimetre User Reduction Facility (SMURF) procedure MAKEMAP. This procedure reduced the noise of the observations while maintaining the source's emission by incorporating a combination of principal component analysis and a maximum likelihood analysis Chapin et al. (2013). Both of these methods have proven useful in reducing bolometer data on their own, but due to the size of raw SCUBA-2 data, specific aspects of each method would result in extreme run times or the process becoming resource intensive.

MAKEMAP broke down the image creation into several steps performed in iteration in order to successfully reduce any background noise Chapin et al.

(2013). The steps used in MAKEMAP were: COM and GAI which remove any common noise features detected by the SQUIDs, EXT to apply extinction corrections, FLT applied a high- and low-pass filters to remove any noise features not removed in the COM and GAI filtering, AST which regrids the data and detects sources to be removed from reduction, the final step is NOI which determines the noise in the gridded map after each step has been performed. A convergence check is then issued and if the check failed the COM, GAI, EXT, and FLT values are inverted and the process is repeated with the inverted values.

In our production of maps, we used the basic conifguration file dimmconfig_bright_compact.lis and altered the AST and FLT sections of the image creation by introducing a mask made from Herschel's 250μm map. The purpose of the map was to exclude the target from interfering with the noise minimization as well as prohibit any emission from the galaxy to be significantly altered during image production. The filter size of the high-pass filter was also modified and an appropriate value was determined to be 175". The maps were returned from MAKEMAP in units of pW with a pixel size of 2" by 2" for both the 450μm and 850μm.

The finalized 450μm image was then re-gridded down to a 4" by 4" pixel grid, and a flux calibration value of 491000 and 4710 were applied to convert from pW to mJy/beam and mJy/square arcsecond respectively. The 850μm maps were re-gridded to an 8" by 8" pixel size and used flux calibration values of 537000 and 2340 for mJy/beam and mJy/square arcsecond . For an easier analysis, the images were also converted to Jy/pixel by multiplying the

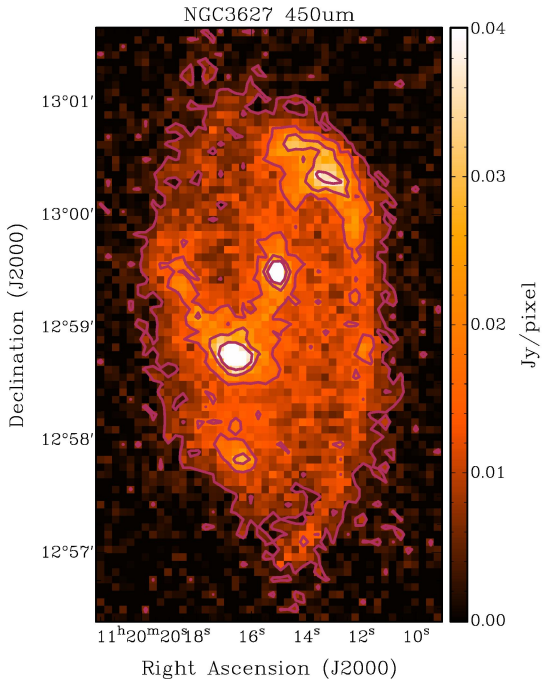

Figure 2.1 450μm observation produced at the end of the image production.

mJy/square arcsecond by 0.001/pixel area. Both the 450μm and 850μm are shown in figures 2.2 and 2.2. The calibration values were determined from observations of Uranus. The overall noise in the finalized image scan be seen in table 2.1.

2.2.1 Beam Shape of the 450μm and 850μm

The Uranus calibration images were also used in determining the shape of the beam for the 450μm and 850μm observations. The beam shape of both the 450μ and 850μm deviate from a single gaussian due to the second maximum of the airy diffraction pattern in the response function of the telescope. This

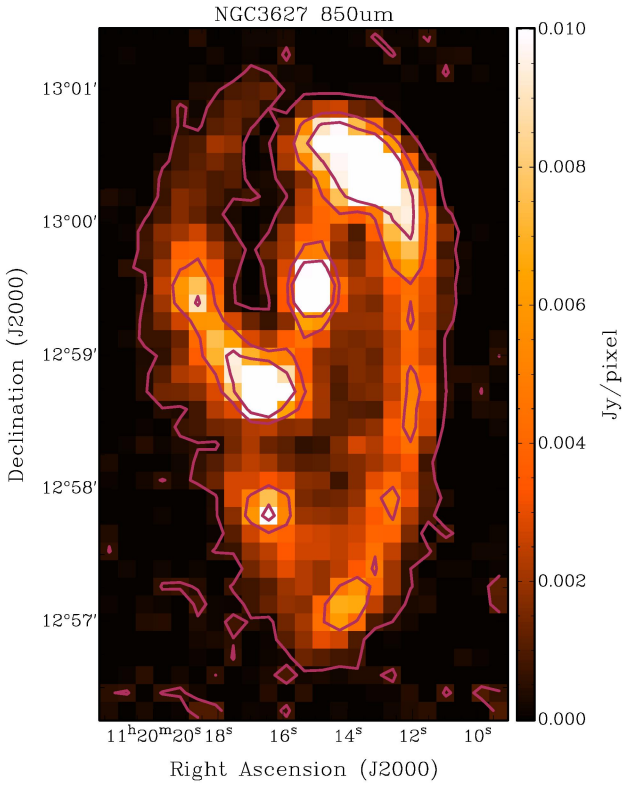

Figure 2.2 850μm observation produced at the end of the image production.

Table 2.1. Properties of NGC3627 SCUBA-2 Observations

Observation	Beam Properties				RMS
	α	θ_α	β	θ_β	*[Jy / Pixel]*
450μm	0.854	7.48″	0.146	23.1″	3.42e-3
850μm	0.962	12.8″	0.038	44.5″	4.76e-4

abnormality was best represented by a sum of two gaussians whose amplitude totals to unity Dempsey et al. (2013). The average beam resolution for the 450μm and 850μm are reported in table 2.1 and match the values within error found in Dempsey et al. (2013). The calibration images and beams can be seen in figures **??** and **??**. The contribution of the error beam in the 850μm emission was negligible and allowed for the beam to be approximated by a single gaussian however the contribution of the error beam in the 450μm images was large enough to require special treatment.

In order to accommodate the 450μm's error component, we used a method employed by another SCUBA-2 survey, the Gould-Belt Survey team. This method utilized the distributive nature of the Fourier transform to create similar error components in the beam resolutions we were convolving to and from. This relationship is shown in equation 2.1 where X_{desire} is the beam width of the resolution we are convolving to, α is the amplitude of the main beam of the 450μm emission, β is the amplitude of the 450μm error beam, X_α and X_β are the main and error beam of the 450μm observations, and $X_{450\mu m}$ is the composition of X_α and X_β beams.

$$(X_{desire} * X_\alpha) * \alpha + (X_{desire} * X_\beta) * \beta = X_{450\mu m} * X_{desire} \tag{2.1}$$

2.3 Ancillary Data

The science goals of this thesis required data outside the capabilities of SCUBA-2. For instance, accurtely determining the dust mass involved fitting

the spectral energy distribution (SED) for NGC3627. To successfully fit an SED, we needed shorter wavelength data to fully probe the cold component of this galaxy. We used data ranging from 100μm to 500μ from the KINGFISH survey Kennicutt et al. (2011) to gain a large enough wavelength range for fitting the cold component. Secondly, the bandpass of the 850μm emisison contains the $CO_{j=3-2}$ transmission line. In order to get a valid approximation on the dust mass, this contribution had to be removed. We used emmisison data from the NGLS using HARP instrumentation on the JCMT Wilson et al. (2012). When a dust mass was obtained, we used $CO_{j=1-0}$ from the Nobeyama 45-m telescope (Kuno et al. (2007)), $CO_{j=2-1}$ from HERACLES (Leroy et al. (2009)), and HI observations from THINGS (Walter et al. (2008)) to determine an reasonable molecular hydrogen mass to approximate a dust-to-gas ratio.

Due to the combination of methods used in MAKEMAP, small scale/extended structure is removed from the final SCUBA-2 images. However, in all of our ancillary data the small scale emission was present in the initial maps. The removal of the extended features from our support data was carried out by converting the images from their native units into pW using the 850μm flux calibration factor or by introducing a scaling factor. The images were overlaid on the original scans as a fakesource and passed through the reduction process. The original scan was then subtracted from the scan with the fakesource present and the residual of the process was the ancillary data with its extended structure removed.

2.3.1 Key Insights on Nearby Galaxies: a Far-Infrared Survey with Herschel (KINGFISH)

The Key Insights on Nearby Galaxies: a Far-Infrared Survey with Herschel (KINGSFISH) was designed to be a follow up to the Spitzer Infrared Nearby Galaxies Survey (SINGS) **?** with observations of the warm and cold component of dust emission using the increased resolution from Herschel Kennicutt et al. (2011). The main science goals of the KINGFISH survey were to better understand the processes of star formation that were shielded by dust, resolved studies of heating and cooling of the interstellar medium (ISM), and to build an inventory of how cold dust emission relates to other dust components in the ISM Kennicutt et al. (2011). The survey consisted of studying 61 nearby galaxies (d<30Mpc) that cover a range of environments each observed at 70μm, 100μ, 160μm, 250μm, 350μm, and 500μm.

We were interested in fitting the cold component of NGC3627's SED, hence we omitted the 70μm emission, and used the 100μm, 160μm, 250μm, 350μm and 500μm. Since the Kingfish data was acquired by a space-based telescope, a significant amount of small scale emission was recovered due to the lack of interference from the atmosphere. The small scale emission was removed by treating the KINGFISH data as a fakesource in the image reduction process. The first step to successfully incorporating the data as a fakesource was to convert the 250μm, 350μm, and 500μm from MJy/sr to mJy/square arcsecond, and similarly the 100μm and 160μm from Jy/pixel to mJy/square arcsecond. After the unit conversion, the 850μm flux calibration factor was applied in reverse, and the new image was then scaled down to better mimic the 850μm

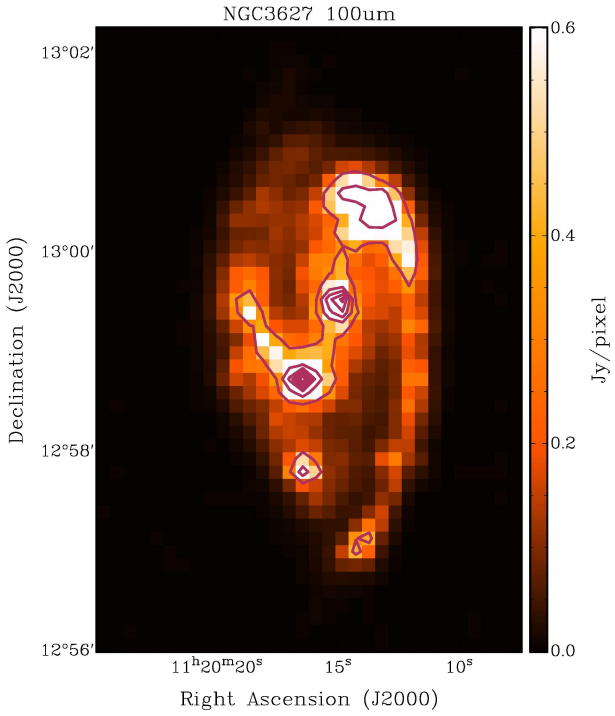

Figure 2.3 Residual of the MAKEMAP filtering of 100μm observations.

emission. After these steps the image was passed into MAKEMAP and treated as an 850μm image. The final data output were gridded to 8" x 8" pixels and can be seen in figures **??** to **??**. The beam size and rms for each image after it has been passed through make map can be seen in table 2.2.

2.3.2 Nearby Galaxy Legacy Survey (NGLS)

The Nearby Galaxy Legacy Survey is an HI-selected set of 155 galaxies contained in the annulus of $2Mpc \leq r \leq 25Mpc$ using the instrumentation aboard the JCMT Wilson et al. (2012). The NGLS contains data observed in several wavelengths that include the 450μm and 850μm data used for this

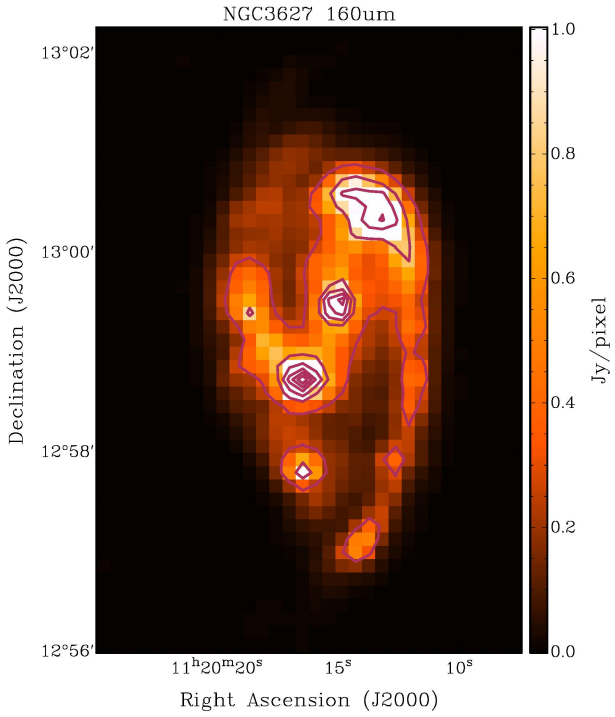

Figure 2.4 Residual of the MAKEMAP filtering of 160μm observations.

Table 2.2. Properties of NGC3627 KINGFISH Observations

Observation	Beam Properties θ_{beam}	RMS *[Jy/Pixel]*	Percentage of Emission Removed
100μm	6.8″	2.24e-3	16.7%
160μm	11.6″	3.95e-3	18.8%
250μm	18.0″	2.47e-3	19.9%
350μm	24.9″	1.08e-3	21.8%
500μm	36.0″	3.87e-4	27.7%

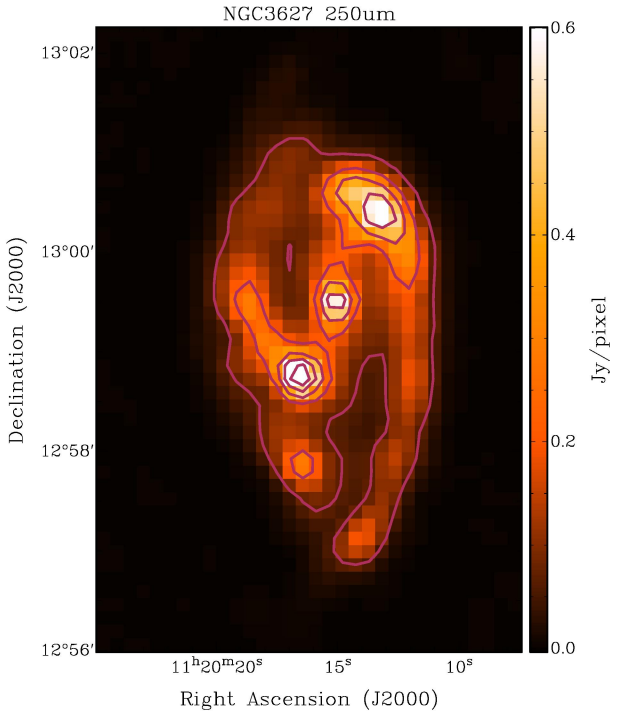

Figure 2.5 Residual of the MAKEMAP filtering of 250μm observations.

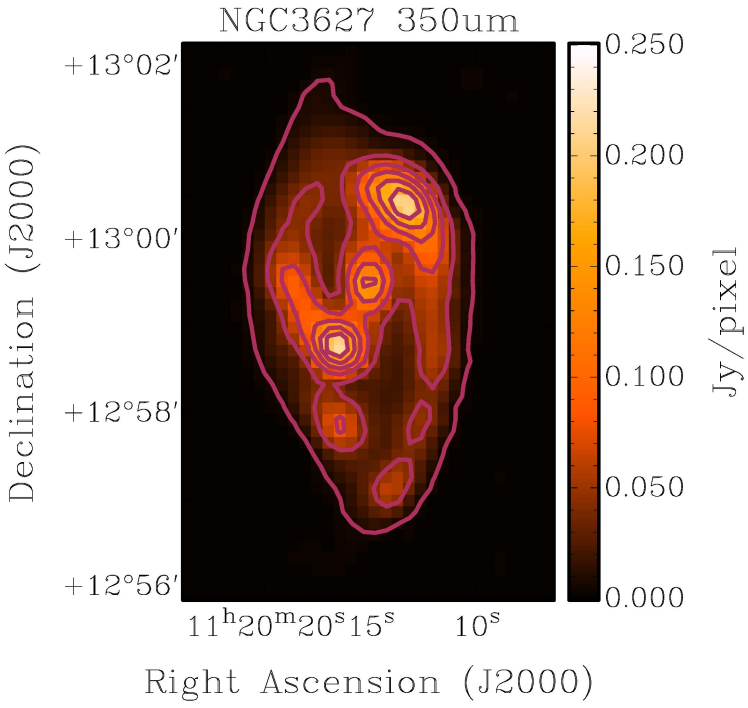

Figure 2.6 Residual of the MAKEMAP filtering of the 350μm observations.

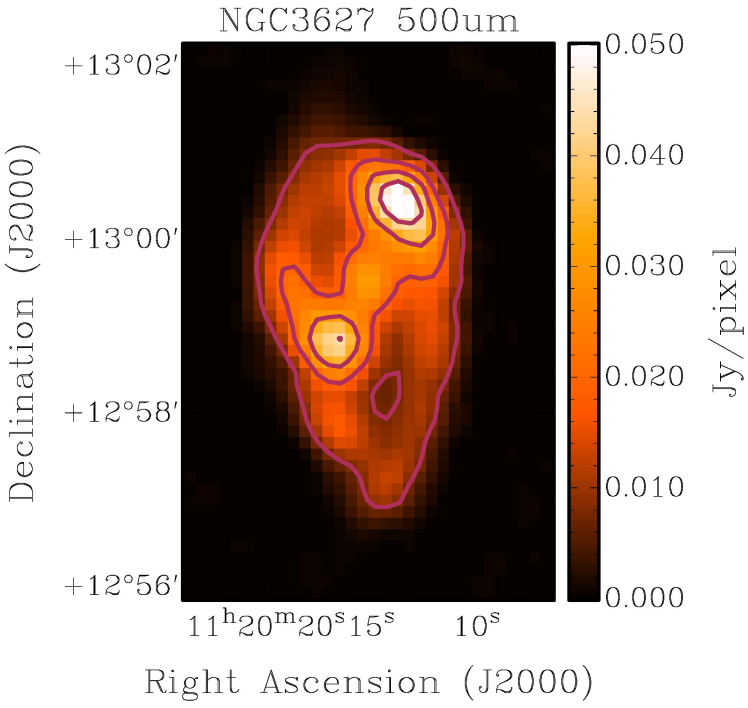

Figure 2.7 Residual of the MAKEMAP filtering of hte 500μm observations.

Table 2.3. Properties of NGC3627 NGLS Observations

Observation	Beam Properties θ_{beam}	RMS *[Jy/Pixel]*	Percentage of Emission Removed
$CO_{j=3-2}$	$14.5''$	1.28e-5	29.8%

thesis. As mentioned previously, the bandpass for SCUBA-2's 850μm emission contains the $CO_{j=3-2}$ line which is contained in the NGLS data set. We used the zeroth moment $CO_{j=3-2}$ maps from the NGLS to determine the percentage of $CO_{j=3-2}$ emission present in the 850μ band as well as removing it for an accurate SED analysis.

Removing the molecular gas contamination from the 850μm images required passing the data through MAKEMAP in a similar manner as the KINGFISH data. The only significant difference was converting the $CO_{j=3-2}$ data from $K * km/s$ to pW. The change of units was done using conversion factor of 0.70 $[K * km/s][mJy/beam]^{-1}$ found by Drabek et al. (2012) for the task of converting HARP data to SCUBA-2 data. The final image product can be seen in figure 2.3.2. We found the average ratio of $CO_{j=3-2}$ to 850μm to be around 29% with some regions dropping to less than 6%. The amount of flux removed and the filtered image's rms can be found in table 2.3.

2.3.3 Nobeyama 45-m

Determining a dust-to-gas ratio required the need for a molecular tracer to estimate the amount of molecular hydrogen present. The most frequently

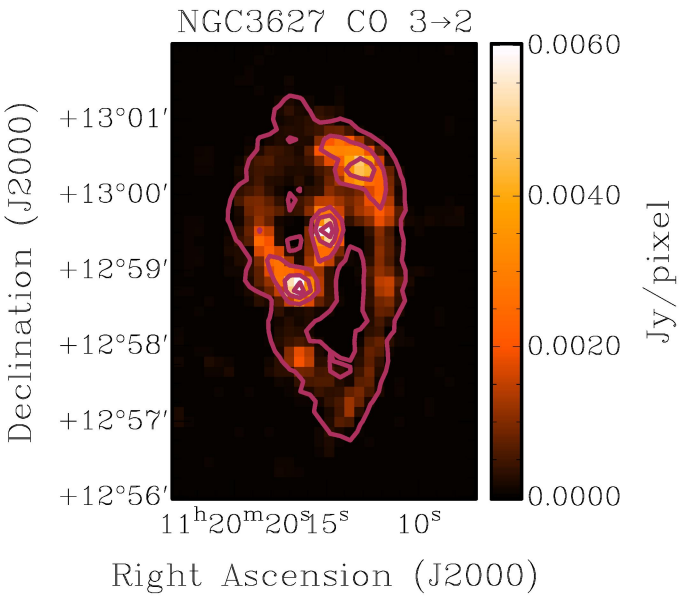

Figure 2.8 Residual of the MAKEMAP filtering of $CO_{j=3-2}$ observations.

Table 2.4. Properties of NGC3627 Nobeyama 45-m Observations

Observation	Beam Properties θ_{beam}	RMS *[K km/s]*	Percentage of Emission Removed
$CO_{j=1-0}$	$15.0''$	0.681	25.8%

used tracer is $CO_{j=1-0}$ due to it's abundance in the ISM. The $CO_{j=1-0}$ we used was taken from the Nobeyama 45-m CO Atlas of Nearby Spiral Galaxies and observed to better understand the roll of bars relating to molecular gas Kuno et al. (2007). The Nobeyama 45-m CO Atlas consists of galaxies ranging from Sa to Scd, located less that 25Mpc from the Milky Way, inclination values greater that 79°, 100μm flux greater than 10Jy, and spiral structure that has not be comprimised through interactions observed with the Nobeyama 45-m telescope (Kuno et al. (2007))

Preparation for the $CO_{j=1-0}$ was performed in a similar matter to the previous ancillary data sets, however instead of determining a direct conversion factor the zeroth moment map was scaled down by a factor 0.001. The scaling factor used was used in lieu of the unit conversion method so the final image would be in it's native units of $[Kkm/s]$. The scaling factor was determined so the input image for the fakesoure would be on the same scale as the 850μm image it was being added onto. The scaling factor was then re-applied as the flux calibration factor to return the original map into its original magnitude. The beam sizes and rms of the filterd $CO_{j=1-0}$ map are displayed in table 2.4 and the final image product can be seen in figure 2.3.3.

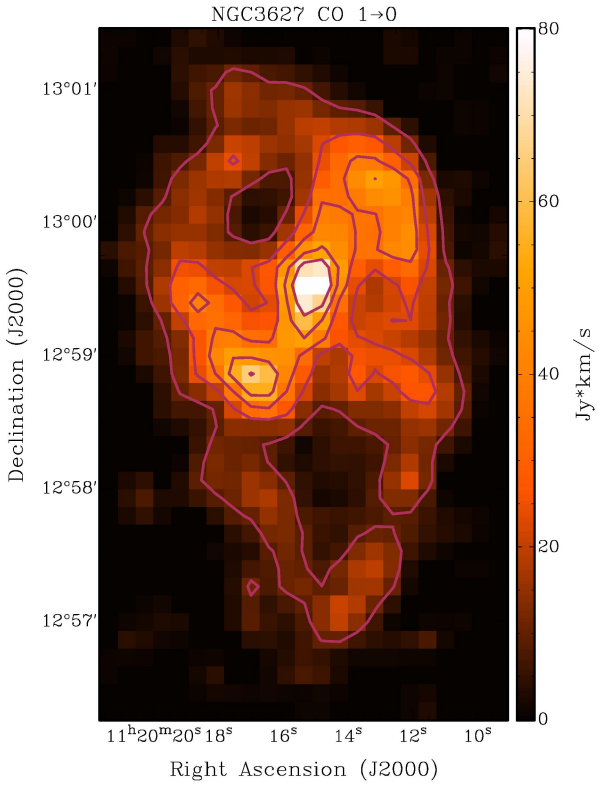

Figure 2.9 Residual of the MAKEMAP filtering of $CO_{j=1-0}$ observations.

Table 2.5. Properties of NGC3627 HERACLES Observations

Observation	Beam Properties θ_{beam}	RMS *[K km/s]*	Percentage of Emission Removed
$CO_{j=2-1}$	$13.0''$	0.305	7.8%

2.3.4 Hetrodyne Reciever Array CO-Line Extragalactic Survey (HERACLES)

The $CO_{j=2-1}$ line was used to determine a $2-1/1-0$ line ratio which can be used to trace a gradient in α_{CO} and hint towards regions of high star-formation Reuter et al. (1996). We used the $CO_{j=1-0}$ data from the Nobeyama 45-m telescope (**??**), and $CO_{j=2-1}$ from the Hetrodyne Reciever Array CO-Line Extragalactic Survey (HERACLES) using the IRAM 30-m telescope. The main goal of HERACLES was to quantify the relationship between atomic and molecular gas and star formation using a large sample of galaxies (Leroy et al. (2009)). The sample of galaxies chosen were targets contained in THINGS that were within observing limits of the IRAM 30-m telescope.

The HERACLES data was treated in the same manner as the Nobeyama 45-m when filtering was applied. Since both the $CO_{j=1-0}$ and $CO_{j=2-1}$ were on the same order of magnitude, the same scaling factor of 0.001 was applied before and after the filtering. The final image can be seen in figure 2.3.4 and the image properties can be seen in table 2.5.

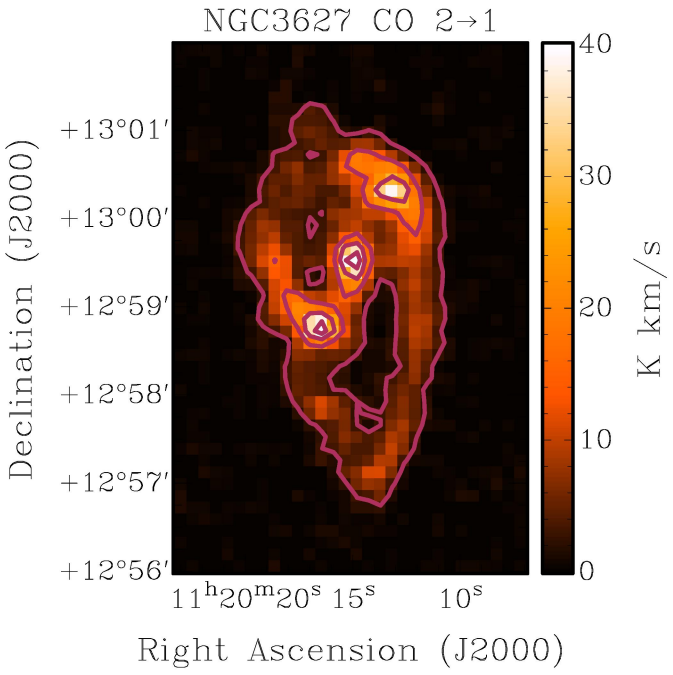

Figure 2.10 Residual of the MAKEMAP filtering of $CO_{j=2-1}$ observations.

2.3.5 The HI Nearby Galaxy Survey (THINGS)

To determine the gas to dust ratio we had to determine the total amount of gas present which required both atomic and molecular hydrogen. We approximated the amount of molecular hydrogen present by using $CO_{j=1-0}$, and measured the amount of atomic hydrogen (HI) present. The source of our atomic hydrogen came from The HI Nearby Galaxy Survey (THINGS) designed to observe HI emission in nearby galaxies with the extereme spatial resolution of the Very Large Array (VLA). Targets in THINGS included many of the SINGS targets with the exception of known HI poor sources (E/S0 type galaxies), dynamicaly complex systems (edge-on spirals), and large extended galaxies found in the local group (Walter et al. (2008)).

The preparation of the HI data was similar to the CO filtering in the sense we did not convert the image into pW and let it remain in its native units. The major difference in the HI extended emission filtering was we did not use a flux map for the final processing; instead we used a surface density map as our fakesource. This was due to issues that arose when using the mass formula given in Walter et al. (2008) on the filtered image. Due to the high resolution of the VLA we measured significant losses in flux after filtering. The value for NGC3627 as a whole can be seen in 2.6 as well as the resolution, and rms of the filtered image. The final data product is shown in figure 2.3.5.

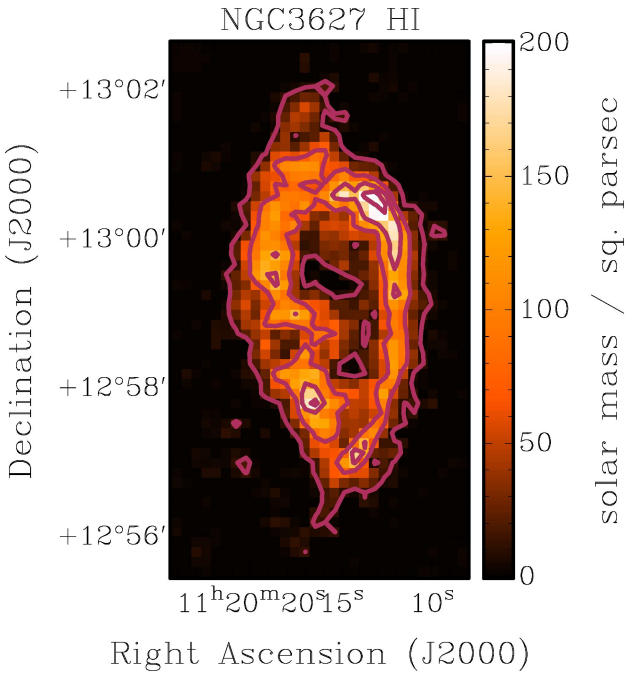

Figure 2.11 Residual of the MAKEMAP filtering of HI observations.

Table 2.6. Properties of NGC3627 THINGS Observations

Observation	Beam Properties			RMS	Percentage of Emission Removed
	θ_{maj}	θ_{min}	θ_{PA}	$[M_\odot/pc^2]$	
HI	10.6″	8.85″	-48.0°	0.760	39.6%

Chapter 3

Results

3.1 Will they ever get here?

Chapter 4

Discussion

4.1 Talk to the hand

Chapter 5

Conclusions

Sandstrom et al. (2013)

Bibliography

Chapin, E. L., Berry, D. S., Gibb, A. G., Jenness, T., Scott, D., Tilanus, R. P. J., Economou, F., & Holland, W. S. 2013, MNRAS, 430, 2545

Dempsey, J. T., Friberg, P., Jenness, T., Tilanus, R. P. J., Thomas, H. S., Holland, W. S., Bintley, D., Berry, D. S., Chapin, E. L., Chrysostomou, A., Davis, G. R., Gibb, A. G., Parsons, H., & Robson, E. I. 2013, MNRAS, 430, 2534

Drabek, E., Hatchell, J., Friberg, P., Richer, J., Graves, S., Buckle, J. V., Nutter, D., Johnstone, D., & Di Francesco, J. 2012, MNRAS, 426, 23

Holland, W. S., Bintley, D., Chapin, E. L., Chrysostomou, A., Davis, G. R., Dempsey, J. T., Duncan, W. D., Fich, M., Friberg, P., Halpern, M., Irwin, K. D., Jenness, T., Kelly, B. D., MacIntosh, M. J., Robson, E. I., Scott, D., Ade, P. A. R., Atad-Ettedgui, E., Berry, D. S., Craig, S. C., Gao, X., Gibb, A. G., Hilton, G. C., Hollister, M. I., Kycia, J. B., Lunney, D. W., McGregor, H., Montgomery, D., Parkes, W., Tilanus, R. P. J., Ullom, J. N., Walther, C. A., Walton, A. J., Woodcraft, A. L., Amiri, M., Atkinson, D., Burger, B., Chuter, T., Coulson, I. M., Doriese, W. B., Dunare, C., Economou, F., Niemack, M. D., Parsons, H. A. L., Reintsema, C. D., Sibthorpe, B., Smail, I., Sudiwala, R., & Thomas, H. S. 2013, MNRAS, 430, 2513

Kennicutt, R. C., Calzetti, D., Aniano, G., Appleton, P., Armus, L., Beirão, P., Bolatto, A. D., Brandl, B., Crocker, A., Croxall, K., Dale, D. A., Meyer,

J. D., Draine, B. T., Engelbracht, C. W., Galametz, M., Gordon, K. D., Groves, B., Hao, C.-N., Helou, G., Hinz, J., Hunt, L. K., Johnson, B., Koda, J., Krause, O., Leroy, A. K., Li, Y., Meidt, S., Montiel, E., Murphy, E. J., Rahman, N., Rix, H.-W., Roussel, H., Sandstrom, K., Sauvage, M., Schinnerer, E., Skibba, R., Smith, J. D. T., Srinivasan, S., Vigroux, L., Walter, F., Wilson, C. D., Wolfire, M., & Zibetti, S. 2011, PASP, 123, 1347

Kuno, N., Sato, N., Nakanishi, H., Hirota, A., Tosaki, T., Shioya, Y., Sorai, K., Nakai, N., Nishiyama, K., & Vila-Vilaró, B. 2007, PASJ, 59, 117

Leroy, A. K., Walter, F., Bigiel, F., Usero, A., Weiss, A., Brinks, E., de Blok, W. J. G., Kennicutt, R. C., Schuster, K.-F., Kramer, C., Wiesemeyer, H. W., & Roussel, H. 2009, AJ, 137, 4670

Reuter, H.-P., Sievers, A. W., Pohl, M., Lesch, H., & Wielebinski, R. 1996, A&A, 306, 721

Sandstrom, K. M., Leroy, A. K., Walter, F., Bolatto, A. D., Croxall, K. V., Draine, B. T., Wilson, C. D., Wolfire, M., Calzetti, D., Kennicutt, R. C., Aniano, G., Donovan Meyer, J., Usero, A., Bigiel, F., Brinks, E., de Blok, W. J. G., Crocker, A., Dale, D., Engelbracht, C. W., Galametz, M., Groves, B., Hunt, L. K., Koda, J., Kreckel, K., Linz, H., Meidt, S., Pellegrini, E., Rix, H.-W., Roussel, H., Schinnerer, E., Schruba, A., Schuster, K.-F., Skibba, R., van der Laan, T., Appleton, P., Armus, L., Brandl, B., Gordon, K., Hinz, J., Krause, O., Montiel, E., Sauvage, M., Schmiedeke, A., Smith, J. D. T., & Vigroux, L. 2013, ApJ, 777, 5

Walter, F., Brinks, E., de Blok, W. J. G., Bigiel, F., Kennicutt, Jr., R. C., Thornley, M. D., & Leroy, A. 2008, AJ, 136, 2563

Wilson, C. D., Warren, B. E., Israel, F. P., Serjeant, S., Attewell, D., Bendo, G. J., Butner, H. M., Chanial, P., Clements, D. L., Golding, J., Heesen, V., Irwin, J., Leech, J., Matthews, H. E., Mühle, S., Mortier, A. M. J., Petitpas, G., Sánchez-Gallego, J. R., Sinukoff, E., Shorten, K., Tan, B. K., Tilanus, R. P. J., Usero, A., Vaccari, M., Wiegert, T., Zhu, M., Alexander, D. M., Alexander, P., Azimlu, M., Barmby, P., Brar, R., Bridge, C., Brinks, E., Brooks, S., Coppin, K., Côté, S., Côté, P., Courteau, S., Davies, J., Eales, S., Fich, M., Hudson, M., Hughes, D. H., Ivison, R. J., Knapen, J. H., Page, M., Parkin, T. J., Rigopoulou, D., Rosolowsky, E., Seaquist, E. R., Spekkens, K., Tanvir, N., van der Hulst, J. M., van der Werf, P., Vlahakis, C., Webb, T. M., Weferling, B., & White, G. J. 2012, MNRAS, 424, 3050